International Journal of Heat and Mass Transfer 51 (2008) 5687–5694

Contents lists available at ScienceDirect

International Journal of Heat and Mass Transfer

journal homepage: www.elsevier.com/locate/ijhmt

A microfluidic study of mouse dendritic cell membrane transport properties of water and cryoprotectants

Hsiu-hung Chen [a], Hong Shen [b], Shelly Heimfeld [c], Kenny K. Tran [b], Joanna Reems [d], Albert Folch [a,e], Dayong Gao [a,*]

[a] Department of Mechanical Engineering, University of Washington, Seattle, WA, USA
[b] Department of Chemical Engineering, University of Washington, Seattle, WA, USA
[c] Bone Marrow Transplant Program, Fred Hutchinson Cancer Research Center, Seattle, WA, USA
[d] Puget Sound Blood Center, Seattle, WA, USA
[e] Department of Bioengineering, University of Washington, Seattle, WA, USA

ARTICLE INFO

Article history:
Received 27 September 2007
Received in revised form 4 April 2008
Available online 4 June 2008

Keywords:
Dendritic cell
Immunotherapy
Microfluidic perfusion system
Soft lithography
PDMS
Monolayer

ABSTRACT

Dendritic cells (DCs) are antigen presenting cells that have been increasingly used in immunotherapy treatment of various diseases and have a great potential for cancer vaccine preparation. Cryopreservation and banking of DCs is critical to facilitate flexible and effective immunotherapy treatment. Therefore, determination of water and cryoprotectant transport properties of DC membrane is indispensable for developing optimal conditions for DCs cryopreservation. Using mouse DCs (mDCs), membrane transport properties were investigated using a microfluidic perfusion system which has recently been developed and fabricated by soft lithography. Cells in the microfluidic system were perfused with various hyperosmotic solutions in the presence or absence of cryoprotectant. The kinetics of cell volume changes under various extracellular conditions were monitored by a video camera and analyzed using a biophysical model to determine water and cryoprotectant transport properties of the cell membrane as well as associated activation energies. It was also shown from this study that the microfluidic perfusion system readily allowed us to: (1) quickly change or manipulate extracellular environment of cells; (2) confine cells in a monolayer channel which prevents imaging ambiguity; and (3) study cell membrane transport kinetics and properties.

1. Introduction

Dendritic cells (DCs) are antigen presenting cells that have been increasingly used in immunotherapy for patients with cancer or other diseases [1–5]. *Ex vivo* manipulation, such as culturing, differentiating and antigen loading, of DCs are crucial aspects for vaccine preparation [6,7]. However, the generation of large quantities of clinical grade DCs is a time-consuming and cost-intensive procedure, which limits the feasibility of repeated vaccinations [8]. Therefore, after the production of sufficient numbers of DCs, the ability to freeze and thaw aliquots of identical DCs can reduce the time and effort involved and also can reduce variability among batches [8–13].

During the freezing, warming, addition or removal of cryoprotective agents (CPA), cells experience a series of highly anisotonic conditions, which can cause lethal injury to cells [14]. In order to obtain optimal protocols for the addition and removal of CPAs and optimal cooling or thawing rates for a given cell type, several important cell membrane transport properties need to be determined. These biophysical properties are: (1) cell membrane permeability coefficients of water (L_p) and of CPAs (P_s), (2) reflection coefficients (σ) of the cell membrane to CPAs, and (3) the activation energies of all of these permeability coefficient (Ea) [14–20]. As far as we know, little work has been done to understand these biophysical properties for DCs. Sukhorukov and his colleagues [21] have analyzed the volume regulation and electric properties of human DCs and Karpas tumor cell line, in order to optimize the protocol for dendritic-tumor electrofusion at room temperature. However, the observation of cell membrane permeabilities of water or CPAs at a single temperature makes it insufficient to predict optimal protocols, which depends on the activation energy of water and CPAs, for cryopreserving DCs.

In this present study, a mouse dendritic cell (mDC) line has been used as a model system to investigate the osmotic behavior of DCs towards water and CPAs at different temperatures. Research on mDCs can serve as an experimental model that will lend insight to clinical trials with human DCs [13,22]. Cell membrane transport properties of rat basophilic leukemia (RBL) were measured in a microfluidic perfusion system recently described [23]. The central

* Corresponding author. Tel.: +1 206 543 1411; fax: +1 206 685 8047.
E-mail address: dayong@u.washington.edu (D. Gao).

0017-9310/$ - see front matter © 2008 Elsevier Ltd. All rights reserved.
doi:10.1016/j.ijheatmasstransfer.2008.04.013

Nomenclature

A	area, μm^2
B	time constant, 1/s
C	concentration, Osm/kg(water)
D	concentration, Osm/kg(water)
Ea	activation energy, kcal/mol
h_1	height of slit, μm
h_2	height of microchannel, μm
L_p	membrane permeability of water, μm/(atm · min)
N	number of osmoles
P_s	membrane permeability of CPA, cm/min
r	correlation coefficient
R	universal gas constant, 0.08207 atm L/(mol K)
T	absolute temperature, K
V	volume, μm^3
$\overline{V}$	volume, μm^3
V_b	osmotically-inactive volume, μm^3
Φ	diameter, μm
σ	reflection coefficients of cell membrane to CPA

Subscripts

c	total cellular
n	non-permeating solute
o	initial state
s	permeating solute

Superscripts

e	extracellular
i	intracellular

idea of using the device is to directly observe, trace, and analyze the volume changes of single cells in anisotonic environments under light microscopy. In order to precisely control the local temperature of the environment of interest, a temperature-controlled system with an optically transparent chamber has been developed and embedded in the microfluidic perfusion system. The benefits of this system are: (1) cost-effectiveness, disposability, reducing labor requirements including washing and reassembling chamber parts, for multiple usages, and (2) ability to customize the needed size and geometry of the chamber with just a change of the mask. In the following sections, we describe the experimental details and present how the understanding of osmotic behaviors for mDCs can benefit the development of efficient cryopreservation protocols.

2. Materials and methods

2.1. Source of cells

Mouse dendritic cells (mDC line) were a gift from Dr. K.L. Rock (Department of Pathology, University of Massachusetts Medical School, MA). Cells were grown in complete RPMI 1640 medium (10% fetal bovine serum, 2 mM L-glutamine, 100 μg/ml streptomycin, and 100 U/ml penicillin) supplemented with non-essential amino acid (100 μM) and 2-mercaptoethanol (50 μM). Cells were maintained in an incubator at 37 °C in a humidified atmosphere containing 5% CO_2.

2.2. Preparation of cell suspensions

On the day of the experiment, mDCs of diameters in the range of 10–15 μm were collected, counted by a hemacytometer, centrifuged, and resuspended in 1× phosphate buffered saline (PBS) (300 mOsm) at a cell density of about 5×10^4/mL, and used within 3 h.

2.3. Design and fabrication for microfluidic perfusion system

Microfluidic devices fabricated in poly(dimethylsiloxane) (PDMS) using soft lithographic techniques have many advantages over conventional systems [24–31] and have been employed in the study of the osmotic behavior of cells for years [32–34]. Our design immobilizes single cells while preventing them from forming multiple layers by restricting the volume available above them, as shown schematically in Fig. 1. In region I, the area encompassed by dotted lines represents the microfluidic perfusion chamber: cells flow from inlet (left in this diagram) to outlet (right) and are trapped by a sieving structure, while the fluid keeps flowing downward through the bottom of the microchannel, h_2 confines the movement of cells. To allow cells to flow freely from the inlet to the chamber, h_2 should be larger than the diameter of cells (Φ) but less than $2 \times \Phi$ (to maintain a monolayer of cells in the channel). The height of the slit (h_1), between the bottom of the channel and the block, should be smaller than Φ. We have found that it is optimal to make $h_1 < \Phi/2$ in order to prevent cells from squeezing into the slot. Since Φ ranges from 10 μm to 15 μm, the dimensions for h_1 and h_2 were chosen to be 5 μm and 20 μm, respectively, and the channel width was chosen to be 150 μm wide. In region II, a chamber is formed to allow bulky liquid to flow through (2 liters per minute), in order to locally control the temperature.

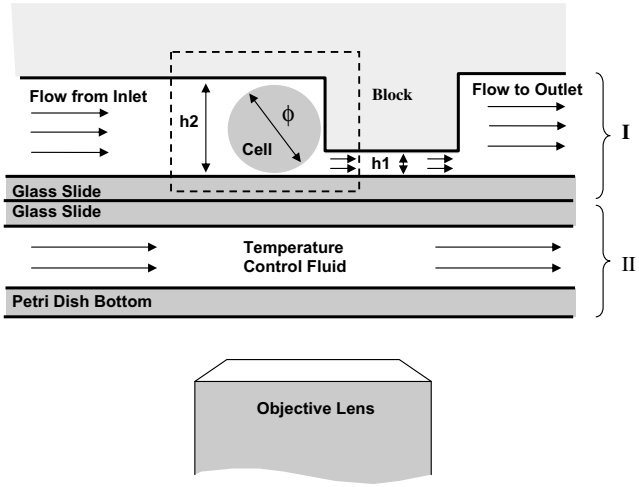

Fig. 1. Schematic diagram showing cell trapped in microfluidic perfusion chamber and monitored through microscope, when the temperature is controlled locally. The solutions are allowed to flow through the bottom of the sieving structure. Cells, whose diameters are larger than h_1, may hardly pass through.

Fabrication of the microfluidic perfusion chamber, shown in region I of Fig. 1, in PDMS (Sylgard 184, Dow-Corning Corp., Midland, MI) was done by soft-lithographic rapid prototyping and replica molding. Fig. 2 depicts the schematic procedures for manufacturing of microfluidic devices in PDMS. From Fig. 2a to e, rapid prototyping was utilized to make a master containing the necessary microfluidic features. Layouts of the design were created as a computer-aided design (CAD) file using AutoCAD (Autodesk Inc., San Rafael, CA). The CAD file was then sent to be printed onto a 20,000 dpi, high-resolution transparency (CAD/Art Service Inc., Bandon, OR), which served as a plastic photomask. In order to con-

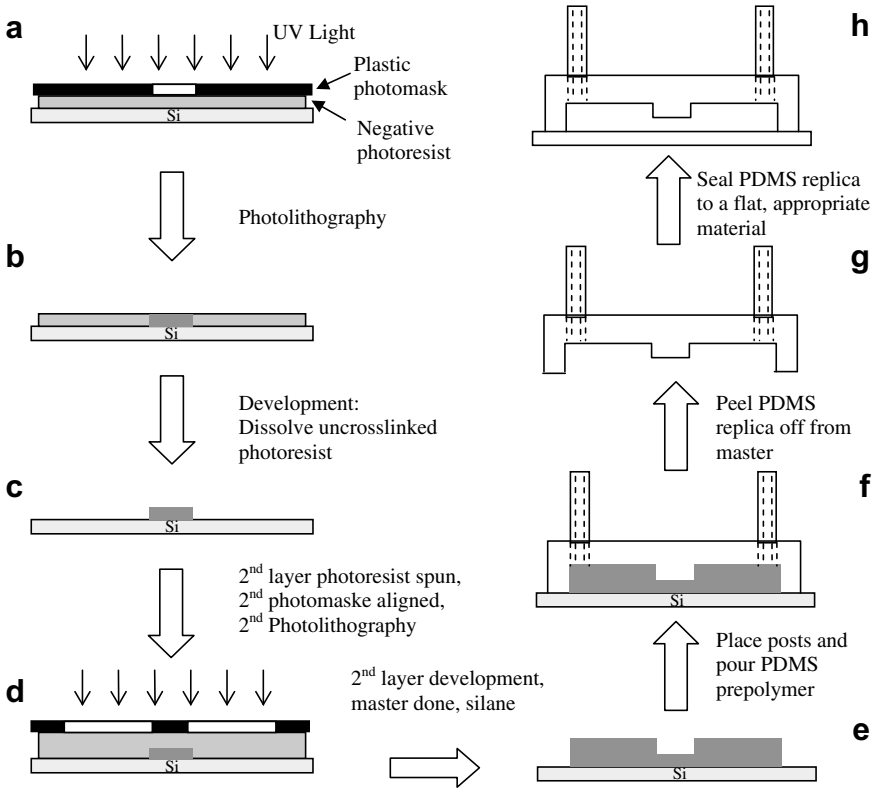

Fig. 2. Fabrication procedures of two-layer microfluidic PDMS device utilizing softlithographic techniques.

struct two-level features, two different layers of photoresist (SU8, MicroChem Corp., Newton, MA) were spin-coated on a 3-in. single-side polished silicon wafer (Montco Silicon Technologies, Spring City, PA). The first layer, spun with SU8-5 at 500 rpm for 10 s and 2950 rpm for additional 30 s, on a silicon wafer was softbaked (to evaporate the solvent and to densify the spin-coated film) and was then exposed to UV light (~3 mJ/cm^2, to polymerize the exposed region) through the photomask for 60 s (Fig. 2a). After being softbaked and developed (Fig. 2b–c), the structure was left on the wafer. The second layer, spun on top of the first with SU8-25 at 500 rpm for 10 s and 2500 rpm for an additional 30 s, was softbaked, UV exposed for 110 s through a different photomask, and then developed, as shown in Fig. 2d and e. Height measurements of structures using Surface Profilometer (Alpha Step 200, KLA-Tencor, San Jose, CA) indicated 3.9 μm and 20.4 μm for h_1 and h_2, respectively. The master was exposed to the vapor of tridecafluouro-1,1,2,2-tetrahydrooctyl-1-trichlorsilane (UCT Inc., Bristol, PA) for ~30 min to prevent bonding between the master surface and the PDMS. Fabrication of the temperature control chamber, shown in region II of Fig. 1, followed similar steps mentioned above, using SU8-100 to construct a thicker layer (~1 mm) instead. The fluidic ports of the device can be applied in two possible ways: (1) two silicone tubes (ID = 1.59 mm, OD = 3.18 mm) which served as inlet and outlet, were glued on the assigned positions before a mixture of PDMS prepolymer and curing agent, 10:1 in weight, was poured over the master (Fig. 2f), or (2) repeat step (1) except glue one silicone tube on the outlet position only, then cutting a cubical hole (approximately 4 mm × 4 mm × 2 mm) for the inlet by hand cutting using a scalpel directly after the PDMS had been cured and placed on a glass slide. After curing in the oven at 65 °C for over two hours, a negative relief made in PDMS of the structure on the master was peeled off (Fig. 2g). To ensure a tight seal, both surfaces of the PDMS device and the substrate (glass slide in this experiment) were exposed to oxygen plasma [35] at room temperature at 150 W for 15 s. Finally, the PDMS device was irreversibly sealed on a glass slide, as shown in Fig. 2h. Fig. 3 shows a photo of this PDMS microfluidic perfusion system. A microfluidic perfusion device (shown individually in Fig. 3a) is lying right on top of a temperature control chamber (Fig. 3b).

2.4. System setup and manipulation procedures

A three-dimension schematic overview of the experimental setup is shown in Fig. 4. The microfluidic perfusion chamber device, made in PDMS and irreversibly sealed on a glass slide, lying on top of the temperature-controlled chamber is mounted on the stage of an inverted microscope (TE2000-S, Nikon, Tokyo, Japan). In order to perform continuous aspiration, a Hamilton Syringe, controlled by a DC motor (out of range and not shown here), was connected through a silicone tube to the outlet of the device. In experiments, 1× PBS was first injected into the inlet to rinse the channel. Due to the oxygen plasma treatment, the surfaces of glass and PDMS inside the channel were highly hydrophilic, and the medium filled the channel quickly. Bubbles formed inside the chamber, but quickly disappeared. The cell suspension was later injected into the same inlet. With continual suction by the Hamilton Syringe, cells flowed through the channel and were trapped in the perfusion chamber. At the same time, part of the cell suspension solution continued moving downstream through the bottom slit. Once the number of cells was enough for the experiment (usually 10–15), the original cell suspension solution was replaced by the new PBS solution with different concentrations of electrolytes (2× and 3×) or 1.5 M Me_2SO solution which is isotonic with respect to NaCl (0.9% NaCl). The new medium was injected in less than half a second in a sufficient volume (0.5 mL) until the silicone tubing (length ~10 mm) or the cubical hole (4 mm × 4 mm × 2 mm) filled so that residual cell suspension (~1 μL) would not affect the desired concentration. The liquid (~1.3 mL) inside the

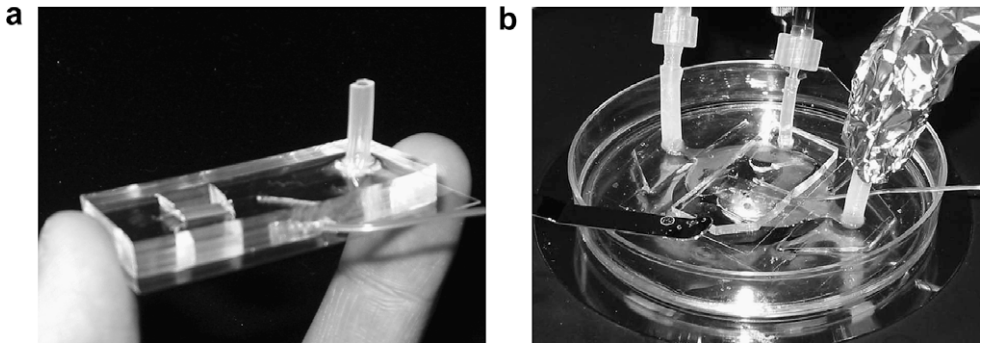

Fig. 3. Microfluidic perfusion system (a) microfluidic structure made of PDMS was irreversibly sealed on a glass slide (b) microfluidic PDMS device was lying right on top of a temperature control chamber.

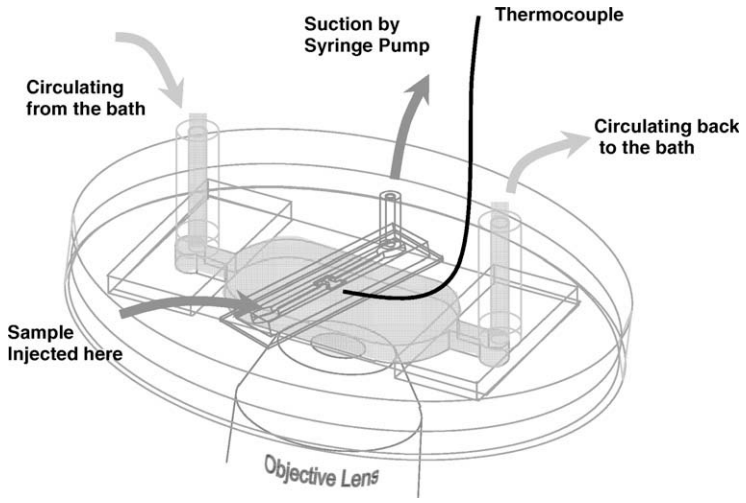

Fig. 4. 3D schematic overview of the experimental setup. Cell suspension and prepared medium with different concentrations were injected into inlet while fluid was sucked continually and automatically from outlet using Hamilton Syringe, controlled by a DC motor. Cell volume response was observed using an inverted microscope throughout the experiment. The local temperature in the neighboring area of the microfluidic perfusion chamber was dominated by the bulky fluid underneath, and monitored by a thermocouple.

chamber of the temperature control device was made from a 1:1, in volume, mixture of distilled water and propylene glycol (CQ Concept Inc., McHENRY, IL), circulated by a circulating bath (PolyScience, Niles, IL). The temperature control device allowed the local temperature around the perfusion chamber to be controlled between −20 °C and 40 °C (±0.5 °C). A T-type thermocouple (SA-1 T, Omega, Stamford, CT) was embedded inside the PDMS near the perfusion chamber for local temperature monitoring. Before, during, and after the perfusion process, the cell volume changes were recorded by a CCD camera (Fusion, Logitech Inc., Fremont, CA), which was connected to the computer, until osmotic equilibrium between the intracellular and extracellular environments was achieved. Shown in Fig. 5a is a top-down view of the microfluidic perfusion chamber; the perfusion chamber is highlighted with dashed lines. Eight cells were clearly trapped within the microfluidic perfusion chamber (Fig. 5b).

2.5. Evaluation of water permeability coefficient

Values of L_p and V_b of the mDCs were determined by measuring changes in cell volume while cells were perfused (in the microfluidic perfusion system) by anisotonic PBS solutions, where only a non-permeating solute was present, using light microscopy. Cell volume was measured from captured cell images by counting the number of pixels of each cell using Matlab (The Mathworks, Inc., Natick, MA). The data were then fitted to the following differential equation to determine L_p, using MLAB (Civilized Software Inc., Silver Spring, MD), which describes the rate of water movement across the cell membrane [36,37]:

$$\frac{dV_c(t)}{dt} = L_p \cdot A \cdot (C_n^i - C_n^e) \cdot R \cdot T \quad (1)$$

The intracellular osmolality during hypertonic shrinkage can be determined using the Boyle van't-Hoff relationship applied to the osmotic responses of cells [38]:

$$C_n^i = C_0 \cdot \left(\frac{V_0 - V_b}{V - V_b}\right) \quad (2)$$

For mDCs, the V_b value was determined by a Boyle van't-Hoff plot [38,39] after cells were perfused and osmotically equilibrated with various PBS solutions with different salt concentrations (2× and 3× isotonic concentration). The L_p values of cells at a specific temperature were determined by least-square curve-fitting [16,38–42] after cells were perfused by 3× PBS solutions.

2.5.1. Determination of CPA permeability of cell membrane: two-parameter transport formalism

When both permeable solute (e.g., permeating CPA) and non-permeating solute (e.g., salts) were present in a solution, the two-parameter transport model can be used to determine L_p and P_s [43,44].

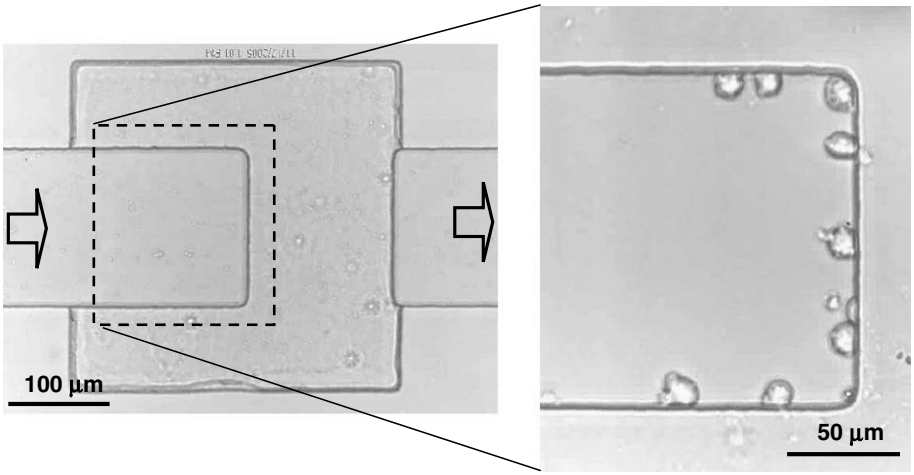

Fig. 5. Top–down view of microfluidic perfusion chamber (a) direction of the flow shown in arrows (b) mDCs were constrained within the chamber.

Compared with Eq. (1), the cell volume change is governed not only by non-permeating solute, but also by the concentration of permeating solutes,

$$\frac{dV_c(t)}{dt} = \frac{dV_s(t)}{dt} + L_p \cdot A \cdot (C^i - C^e) \cdot R \cdot T \tag{3}$$

and the solute flux is given by

$$\frac{dN_s(t)}{dt} = P_s A (C_s^e - C_s^i), \tag{4}$$

$N_s(t)$ and $V_s(t)$ are interchangeable for

$$N_s(t) = V_s(t)/\overline{V}_s \tag{5}$$

The L_p and P_s values of cells at room temperature (22 °C) were determined by least-square curve-fitting after cells were perfused by 1.5 M Me_2SO solution isotonic with respect to NaCl.

The activation energy was calculated using the mean L_p at four different temperatures: 12, 22, 25, and 32 °C

$$\ln(L_p(T)) = -\frac{Ea}{RT} + \text{Constant} \tag{6}$$

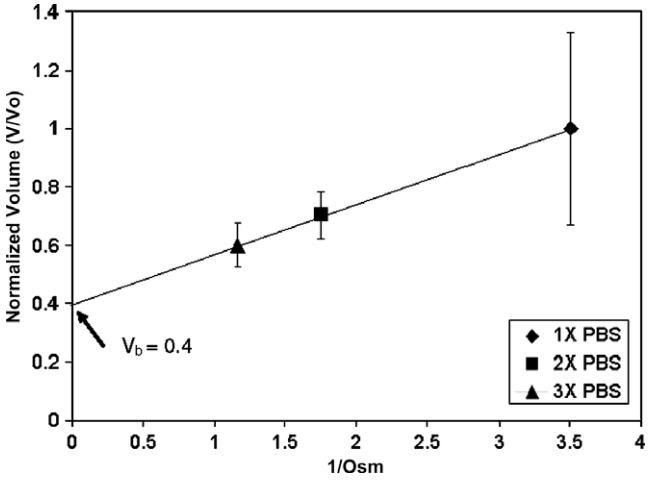

Fig. 6. Boyle Van't-Hoff relationship for mDCs at room temperature (22 °C) by diffusion method. Cells were randomly collected for measurements. Inactive cell volume, V_b, were determined to be 40% of original/isotonic volume.

2.6. Compensation of a time-variant extracellular osmolality

In order to compensate for a non-zero replacement time, we simply replace the constant C^e with a time-variant function,

$$C^e(t) = D \times (1 - e^{-Bt}) \tag{7}$$

For example, D and B will be 0.9 and 1.354, respectively, if cells are perfused with 3× PBS at 400 μm/s (or 1.8 nl/s) and the extracellular environment reaches 90% of its ultimate osmolality [23].

3. Results

3.1. Determination of V_b, L_p, P_s, and Ea

A Boyle van't Hoff plot is shown in Fig. 6. The inactive volume V_b of mDCs was determined to be 40% [n = 15 for each concentration, correlation coefficient (r^2) of 0.99] of the original/isotonic volume, obtained by the diffusion method [38,39]. Fig. 7 shows photographs of mDCs perfused with hypertonic 3× PBS at 22 °C. The arrow depicts where the origin of the flow. Cells were trapped within the perfusion chamber while the medium flowed downstream by suction as shown in Fig. 7a. A magnified view, Fig. 7b, shows a series of photographs where a cell was exposed to the hypertonic solution at t = −10, 0, 10, 20, 35, and 60 s, respectively. The cell decreased in size until it reached the osmotic balance between intracellular and extracellular solutions. The history of volume change of mDC was then processed using Matlab, shown in Fig. 7c. The water permeability coefficient, L_p, was determined by curve-fitting, using Eqs. (1), (2) and (7), as shown in Fig. 8. Other individual cells, perfused at 12, 25, and 32 °C, were processed by the identical method aforementioned. Values of L_p determined at different temperatures were listed in the first major row I of Table 1.

Fig. 9 shows the volume change of cells after being perfused at 22 °C by 1.5 M Me_2SO solution isotonic with respect to NaCl. In Fig. 9b, a series of magnified photographs exhibit a single cell that was exposed to the solution at t = 0, 10, 20, 40, 60, and 80 s, respectively. The history of volume changes of mDC was then processed using Matlab, shown in Fig. 9c. The water permeability coefficient, L_p, and Me_2SO permeability, P_s, of the cells at 22 °C were determined by curve-fitting (using Eqs. (3), (4), (5) and (7)), shown in Fig. 10. Values of L_p and P_s are listed in the second major row II of Table 1.

In Fig. 11, an Arrhenius plot shows the natural logarithm of the average L_p versus the reciprocal of the absolute temperature. The activation energy of water for mDCs was determined by curve-fitting, using Eq. (6), and found to be 2.39 Kcal/mol.

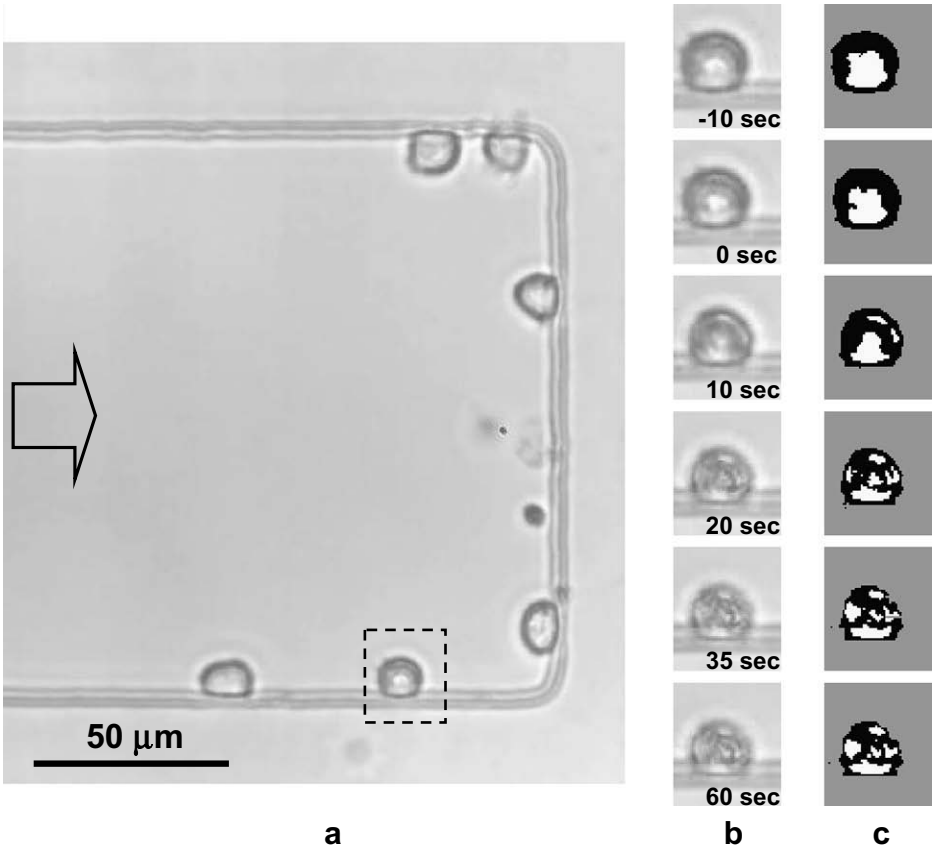

Fig. 7. (a) mDCs trapped within the perfusion chamber, (b) a magnified view inside dashed line when cells were perfused by 3 PBS at the moments of $t = -10$, 0, 10, 20, 35, and 60 s, respectively, (c) post-processed images corresponding laterally to (b).

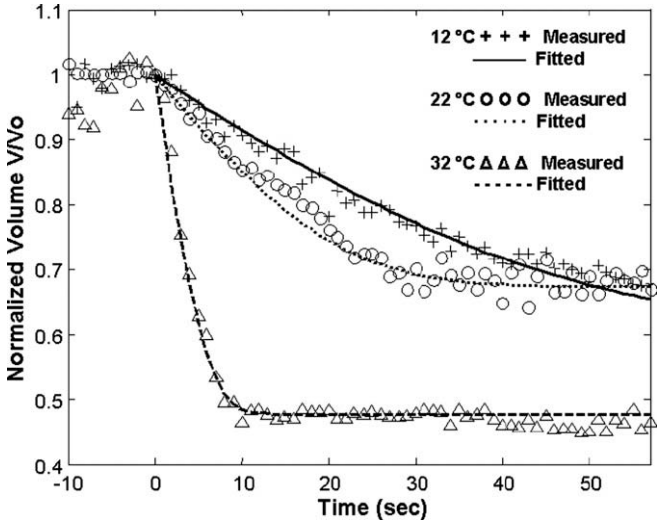

Fig. 8. Volume change of mDCs in response to 3× PBS.

Table 1
Water permeability (L_p) at four different temperatures and Me_2SO permeability (P_s) at room temperature

	Temperature (°C)	L_p (μm/min/atm)	P_s (10^{-3} cm/min)
		Mean ± SD (n, r^2)	Mean ± SD (n, r^2)
I. (3× PBS)	12	0.11 ± 0.02 (8, >0.87)	N/A
	22	0.16 ± 0.03 (4, >0.83)	N/A
	25	0.95 ± 0.29 (6, >0.93)	N/A
	32	1.54 ± 0.66 (6, >0.90)	N/A
II. (1.5 M DMSO + 0.9% NaCl)	22	0.17 ± 0.04 (5, >0.66)	0.63 ± 0.29 (5, >0.66)

4. Discussion and conclusion

This study was undertaken to explore the unknown fundamental cryobiologic characteristics of mammalian DCs by microfluidic systems. Previous works associated with cryopreserving DCs have been conducted by either trial-and-error or by experienced protocols [8,9,11–13]. With the understanding of the biophysical properties of DCs, increased viability of freezing/thawing DCs may be achieved.

The microfluidic perfusion chamber made in PDMS using soft lithography proved to be useful for confining cells within a perfusion chamber. PDMS is transparent, allowing for light microscopy monitoring of cell volume changes. The osmotic behavior and permeability of cells are temperature-dependent. A temperature-controlled device has been developed and used to control the temperature in the microfluidic perfusion system to study cell permeability at various temperatures, ranging from 12 to 32 °C. By analyzing captured images of cell volume changes during perfusion, inactive cell volume V_b, water permeability coefficient L_p at different temperatures, and Me_2SO permeability coefficient P_s can be determined.

In this study, image processing was utilized to estimate the three-dimensional volume of cells from two-dimensional images captured under a light microscope. The captured images were transferred to eight-bit gray scale photos, and then were processed

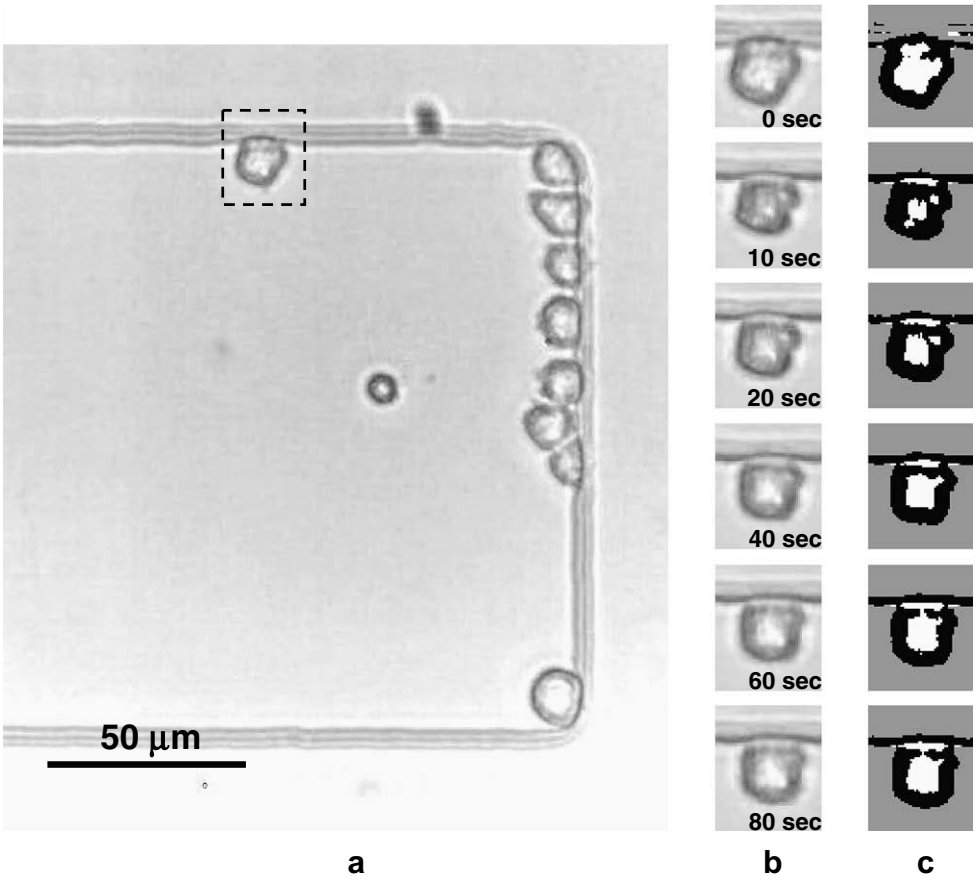

Fig. 9. (a) mDCs trapped within the perfusion chamber, (b) a magnified view inside dashed line when cells were perfused by 1.5 M Me_2SO plus 0.9% NaCl at times t = 0, 10, 20, 40, 60, and 85 s, respectively, (c) post-processed images corresponding laterally to (b).

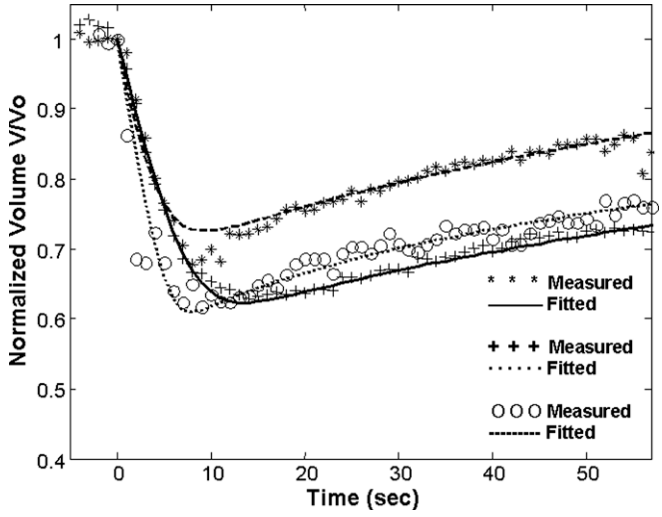

Fig. 10. Volume change of mDCs in response to 1.5 M Me_2SO plus 0.9% NaCl.

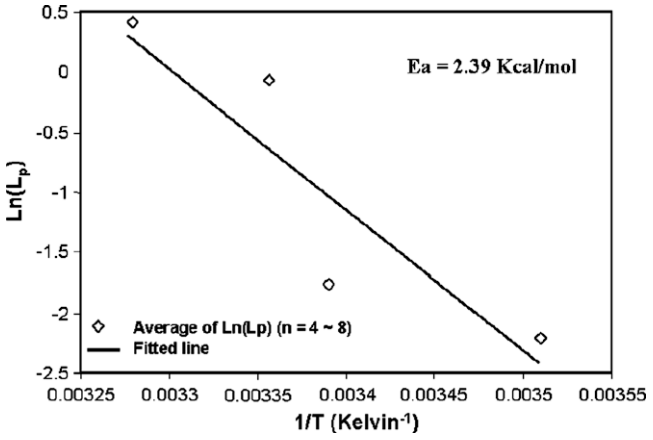

Fig. 11. Arrhenius plot showing the natural logarithms of the average L_p versus the reciprocal of the absolute temperatures. Linear regressions were performed and found to fit the observed data with correlation coefficients (r^2) of 0.80. Activation energies (Ea) of L_p was calculated from the slopes of the regressions.

to enhance their contrast. In the case shown in Fig. 7b, the cell was estimated to occupy 768 pixels as its 2D area after the enhancement of the contrast, shown in Fig. 7c. According to our calibration, one pixel represents an area of 0.37 μm × 0.37 μm under total magnification of 200X. Therefore, the volume obtained from the 2D area measurement is equal to 780 μm^3. Errors may occur when cells are out of focus, so that the boundary between cells and extracellular environment is blurred. These blurry images were not used in the analysis. In some cases, when the difference of grey scale values between cells/medium and cells/PDMS were too small, as shown in Fig. 9c, the shadow formed by the vertical sieving structure (usually has a uniform pattern) may not be efficiently eliminated in order to create clean images, such as the case presented in Fig. 7c. Subtractions of this non-cell portion need to be carefully processed.

Experimental results have also shown that the shape of some cells tend to become irregular during dehydration. This can also introduce errors in analysis since the fundamental assumption of the light microscopy method is based on spherical cellular shapes. A 3D image reconstruction through different focusing planes during perfusion can be a possible solution to obtain more accurate cell volume measurements.

In conclusion, the microfluidic device enables us to: (1) confine individual cells within a monolayer chamber, which prevents imaging ambiguity, such as cells overlapping or moving out of the focus plane; (2) load/unload membrane permeating materials into/from intracellular environments through perfusing extracellularly; (3) readily monitor the changes of extracellular conditions by rapidly perfusing a single cell or a group of cells with prepared media; and (4) study cell osmotic response and determine cell membrane transport properties. In addition, this system is cost-effective and disposable for multiple usages and allows customization of size and geometry of the perfusion chamber with just a change of the photomask for various applications.

Acknowledgement

This work was supported by a grant from NIH FHCRC/UW Center for Medical Countermeasures against Radiation and a Gift grant from the Washington Research Foundation.

References

[1] J.L. Schultz, S. Michalak, M.J. Seamon, G. Dranoff, K. Jung, J. Daley, J.C. Delgado, J.G. Gribben, L.M. Nadler, CD40-activated human B cells: and alternative source of highly efficient antigen presenting cells to generate autologous antigen-specific T cells for adoptive immunotherapy, J. Clin. Invest. (100) (1997) 2757–2765.
[2] J. Banchereau, A.K. Palucka, M. Dhodapkar, S. Burkeholder, N. Taquet, A. Rolland, S. Taquet, S. Coquery, K.M. Wittkowski, N. Bhardwaj, L. Pineiro, R.M. Steinman, J. Fay, Immune and clinical responses in patients with metastatic melanoma to CD34+ progenitor-derived dendritic cell vaccine, Cancer Res. (61) (2001) 6451–6458.
[3] D. Bell, J.W. Young, J. Banchereau, Dendritic cells, Adv. Immunol. 72 (72) (1999) 255–324.
[4] R.M. Dallal, M.T. Lotze, The dendritic cell and human cancer vaccines, Curr. Opin. Immunol. 5 (12) (2000) 583–588.
[5] D. O'Mahony, S. Kummar, M.E. Gutierrez, Non-small-cell lung cancer vaccine therapy: A concise review, J. Clin. Oncol. 35 (23) (2005) 9022–9028.
[6] D.W. O'Neill, S. Adams, N. Bhardwaj, Manipulating dendritic cell biology for the active immunotherapy of cancer, Blood 8 (104) (2004) 2235–2246.
[7] P. Thumann, I. Moc, J. Humrich, T.G. Berger, E.S. Schultz, G. Schuer, L. Jenne, Antigen loading of dendritic cells with whole tumor cell preparations, J. Immunol. Meth. (277) (2003) 1–16.
[8] J. Westermann, I.J. Koerner, J. Kopp, S. Kurz, M. Zenke, B. Doerken, A. Pezzutto, Cryopreservation of mature monocyte-derived human dendritic cells for vaccination: influence on phenotype and functional properties, Cancer Immunol. Immunother. (52) (2003) 194–198.
[9] J. John, A. Dalgleish, A. Melcher, H. Pandha, Cryopreserved dendritic cells for intratumoral immunotherapy do not require re-culture prior to human vaccination, J. Immunol. Meth. (299) (2005) 37–46.
[10] H.S. Pandha, R.J. John, J. Hutchinson, N. James, M. Whelan, C. Corbishley, A.G. Dalgleish, Dendritic cell immunotherapy for urological cancers using cryopreserved allogeneic tumour lysate-pulsed cells: a phase I/II study, BJUI (94) (2004) 412–418.
[11] J. Seager Danciger, M. Lutz, S. Hama, D. Cruz, A. Castrillo, J. Lazaro, R. Phillips, B. Premack, J. Berliner, Method for large scale isolation, culture and cryopreservation of human monocytes suitable for chemotaxis, cellular adhesion assays, macrophage and dendritic cell differentiation, J. Immunol. Meth. 1–2 (288) (2004/5) 123–134.
[12] B. Feuerstein, T.G. Berger, C. Maczek, C. Roeder, D. Schreiner, U. Hirsch, I. Haendle, W. Leisgang, A. Glaser, O. Kuss, T.L. Diepgen, G. Schuler, B. Schuler-Thurner, A method for the production of cryopreserved aliquots of antigen-preloaded, mature dendritic cells ready for clinical use, J. Immunol. Meth. (254) (2000) 15–29.
[13] T. Sai, S.W.F. Milling, B. Mintz, Freezing and thawing of bone marrow-derived murine dendritic cells with subsequent retention of immunophenotype and of antigen processing and presentation characteristics, J. Immunol. Meth. (264) (2002) 153–162.
[14] P. Mazur, Equilibrium, quasi-equilibrium, and nonequilibrium freezing of mammalian embryos, Cell Biophys. 1 (17) (1990) 53–92.
[15] F.G. Arnaud, D.E. Pegg, Permeation of glycerol and propane-1,2-diol into human platelets, Cryobiology 2 (27) (1990) 107–118.
[16] D.Y. Gao, J. Liu, C. Liu, L.E. Mcgann, P.F. Watson, F.W. Kleinhans, P. Mazur, E.S. Critser, J.K. Critser, Prevention of Osmotic Injury to Human Spermatozoa during Addition and Removal of Glycerol, Human Reproduct. 5 (10) (1995) 1109–1122.
[17] J.B. Heymann, P. Agre, A. Engel, Progress on the structure and function of aquaporin 1, J. Struct. Biol. 2 (121) (1998) 191–206.
[18] L.E. Mcgann, M. Stevenson, K. Muldrew, N. Schachar, Kinetics of Osmotic Water-Movement in Chondrocytes Isolated from Articular-Cartilage and Applications to Cryopreservation, J. Orthopaedic Res. 1 (6) (1988) 109–115.
[19] K. Muldrew, L.E. Mcgann, The osmotic rupture hypothesis of intracellular freezing-injury, Biophys. J. 2 (66) (1994) 532–541.
[20] M. Toner, E.G. Cravalho, M. Karel, Thermodynamics and kinetics of intracellular ice formation during freezing of biological cells, J. Appl. Phys. 3 (67) (1990) 1582–1593.
[21] V.L. Sukhorukov, R. Reuss, J.M. Endter, S. Fehrmann, A. Katsen-Globa, P. Gessner, A. Steinbach, K.J. Mueller, A. Karpas, U. Zimmermann, H. Zimmermann, A biophysical approach to the optimisation of dendritic-tumour cell electrofusion, Biochem. Biophys. Res. Commun. (346) (2006) 829–839.
[22] P. Rawson, I.F. Hermans, S.P. Huck, J.M. Roberts, H. Pircher, F. Ronchese, Immunotherapy with dendritic cells and tumor major histocompatibility complex class I-derived peptides requires a high density of antigen on tumor cells, Cancer Res. 16 (60) (2000) 4493–4498.
[23] H. Chen, Jester, J.P. Purtteman, S. Heimfeld, A. Folch, D. Gao, Development of a microfluidic device for determination of cell osmotic behavior and membrane transport properties, Cryobiology 3 (55) (2007) 200–209.
[24] R.W. Applegate, J. Squier, T. Vestad, J. Oakey, D.W.M. Marr, Optical trapping, manipulation, and sorting of cells and colloids in microfluidic systems with diode laser bars, Opt. Express 19 (12) (2004) 4390–4398.
[25] D.C. Duffy, J.C. McDonald, O.J.A. Schueller, G.M. Whitesides, Rapid prototyping of microfluidic systems in poly(dimethylsiloxane), Anal. Chem. 23 (70) (1998) 4974–4984.
[26] J.M.K. Ng, I. Gitlin, A.D. Stroock, G.M. Whitesides, Components for integrated poly(dimethylsiloxane) microfluidic systems, Electrophoresis 20 (23) (2002) 3461–3473.
[27] J.C. McDonald, D.C. Duffy, J.R. Anderson, D.T. Chiu, H.K. Wu, O.J.A. Schueller, G.M. Whitesides, Fabrication of microfluidic systems in poly(dimethylsiloxane), Electrophoresis 1 (21) (2000) 27–40.
[28] D. Qin, Y.N. Xia, G.M. Whitesides, Rapid prototyping of complex structures with feature sizes larger than 20 mu m, Adv. Mater. 11 (8) (1996) 917.
[29] A. Tourovskaia, X. Figueroa-Masot, A. Folch, Differentiation-on-a-chip: A microfluidic platform for long-term cell culture studies, Lab Chip 1 (5) (2005) 14–19.
[30] G.M. Whitesides, E. Ostuni, S. Takayama, X.Y. Jiang, D.E. Ingber, Soft lithography in biology and biochemistry, Annu. Rev. Biomed. Eng. (3) (2001) 335–373.
[31] Y.N. Xia, G.M. Whitesides, Soft lithography, Ann. Rev. Mater. Sci. (28) (1998) 153–184.
[32] D.A. Ateya, F. Sachs, P.A. Gottlieb, S. Besch, S.Z. Hua, Volume cytometry: microfluidic sensor for high-throughput screening in real time, Anal. Chem. 5 (77) (2005) 1290–1294.
[33] P.H.G. Chao, A.C. West, C.T. Hung, Chondrocyte intracellular calcium, cytoskeletal organization, and gene expression responses to dynamic osmotic loading, Am. J. Physiol.-Cell Physiol. 4 (291) (2006) C718–C725.
[34] D. Huh, W. Gu, Y. Kamotani, J.B. Grotberg, S. Takayama, Microfluidics for flow cytometric analysis of cells and particles, Physiol. Meas. 3 (26) (2005) R73–R98.
[35] J.C. McDonald, D.C. Duffy, J.R. Anderson, D.T. Chiu, H.K. Wu, O.J.A. Schueller, G.M. Whitesides, Fabrication of microfluidic systems in poly-(dimethylsiloxane), Electrophoresis 1 (21) (2000) 27–40.
[36] Hugh Davson, J.F. Danielli (Eds.), The Permeability of Natural Membranes, Cambridge University Press, Cambridge, UK, 1970.
[37] L.E. Mcgann, M. Stevenson, K. Muldrew, N. Schachar, Kinetics of osmotic water-movement in chondrocytes isolated from articular-cartilage and applications to cryopreservation, J. Orthop. Res. 1 (6) (1988) 109–115.
[38] B. Lucke, M. McCutcheon, The living cell as an osmotic system and its permeability to water, Physiol. Rev. (12) (1932) 68–138.
[39] S.P. Leibo, Water permeability and its activation-energy of fertilized and unfertilized mouse ova, J. Membr. Biol. 3 (53) (1980) 179–188.
[40] D.Y. Gao, J.J. Mcgrath, J. Tao, C.T. Benson, E.S. Critser, J.K. Critser, Membrane-transport properties of mammalian oocytes - a micropipette perfusion technique, J. Reprod. Fertil. 2 (102) (1994) 385–392.
[41] J.J. Mcgrath, A microscope diffusion chamber for the determination of the equilibrium and non-equilibrium osmotic response of individual cells, J. Microsc. -Oxf. SEP (139) (1985) 249–263.
[42] J.J. McGrath, Quantitative measurement of cell membrane transport: Technology and applications, Cryobiology 4 (34) (1997) 315–334.
[43] M.H. Jacobs, The simultaneous measurement of cell permeability to water and to dissolved substances, J. Cell. Compar. Physiol. (2) (1933) 427–444.
[44] F.W. Kleinhans, Membrane permeability modeling: Kedem–Katchalsky vs. a two-parameter formalism, Cryobiology 4 (37) (1998) 271–289.